Machine learning-based optimization of a single-element transcranial focused ultrasound transducer for deep brain neuromodulation in mice

Sadman Labib and Jingfei Liu

Department of Mechanical Engineering, Texas Tech University, Lubbock, Texas, USA

E-mail: Jingfei.Liu@ttu.edu

Abstract

Transcranial focused ultrasound is an emerging noninvasive technique for neuromodulation, offering high spatial precision and potential for deep brain penetration. For ultrasound neuromodulation studies in mice, current transducers can successfully reach shallow and middle brain depths; however, accessing deep-brain regions, especially those near the lower skull bone, remains challenging due to skull-induced attenuation, reflection, and acoustic aberration. To address this issue, this study presents a machine learning-based computational framework for optimizing single-element transducer designs to achieve precise deep-brain targeting in a mouse model. This framework includes a surrogate model and an evolutionary optimization approach. The surrogate model, which consists of Random Forest regressor and classifier models, was trained on acoustic simulation results to predict acoustic performance from design parameters. A total of 72 simulations were performed across coronal and sagittal planes, systematically varying parameters of frequency (1-6 MHz), radius of curvature (5-7 mm), and f-number (0.58-1.0). Each design was evaluated using five performance metrics: focal length, focal shape, maximum pressure at the focal region, pressure maximum location, and sidelobe suppression. The surrogate was combined with an evolutionary algorithm, Non-Dominated Sorting Genetic Algorithm II, to perform multi-objective optimization and identify high-performing transducer designs. The optimized design resulted in more compact, symmetric focal regions and accurate energy delivery to deep targets, with minimal off-target exposure, even in the presence of complex skull anatomy. Results indicate that lower f-numbers, moderate radius of curvature, and higher frequencies facilitate precise deep brain targeting. Overall, this data-driven approach enables the effective design of single-element transducers for deep-brain neuromodulation in mice and provides a framework for designing transcranial transducers for other brain targets, potentially accelerating the clinical translation of focused ultrasound technologies.

Keywords: transcranial focused ultrasound, deep brain neuromodulation, single-element ultrasound transducer, hypothalamus, surrogate model, multi-objective optimization, Random Forest, NSGA-II

1. Introduction

Transcranial focused ultrasound (t-FUS) is an emerging technology for noninvasive neuromodulation, offering potential applications across neurology (Lee *et al.*, 2016), psychiatry (Kubanek, 2018; Li *et al.*, 2020; Maria *et al.*, 2024), and research on brain functions (Ham *et al.*, 2024; Legon *et al.*, 2018a; Legon *et al.*, 2018b; Kim *et al.*, 2022) and disorders (Lee *et al.*, 2024). It demonstrates high spatial resolution and deep penetration, making it a valuable tool for modulating neuronal activity in specific brain circuits (Mehic *et al.*, 2014; Niu *et al.*, 2018; Darmani *et al.*, 2022). In contrast, other noninvasive neuromodulation techniques, such as repetitive transcranial magnetic stimulation and transcranial direct current stimulation, lack the capability of targeting deep brain regions (Samoudi *et al.*, 2019a). Preclinical and clinical studies have shown that t-FUS can selectively target specific areas within the central and peripheral nervous systems with remarkable spatial precision, underscoring its potential to advance therapeutic neuromodulation (Fini and Tyler, 2017; Zhang *et al.*, 2021). However, the underlying mechanisms of its therapeutic effects are largely unclear. This complexity arises from the multiple physical and biological interactions among ultrasound waves, skull structure, and brain tissue, combined with the intricate nature of neurological disease pathogenesis. As a result, extensive foundational studies in animal models are crucial to bridging the gap between basic research and clinical applications of t-FUS therapy.

In t-FUS neuromodulation, both phased array and single-element transducers are used(Javid *et al.*, 2023). Phased array transducers offer substantial advantages in spatial resolution, which is critical for precisely targeting specific brain regions. For example, a 16-element phased array has been shown to achieve a lateral resolution of 1.6 mm with a pressure output of 1.15 MPa at a focal depth of 12 mm, providing a high level of precision suitable for deep brain targets(Ilham *et al.*, 2021). Another unique capability of phased arrays is their ability to produce multiple foci simultaneously, allowing for multitarget neuromodulation (Zhuang *et al.*, 2022). The skull's natural distortion of ultrasound waves presents a challenge for t-FUS, but phased array transducers can adaptively compensate for these distortions. By dynamically adjusting the phase and amplitude of each element, phased arrays can maintain a stable focus and consistent intensity through the skull (Kobayashi *et al.*, 2018). This adaptive correction capability helps to optimize acoustic pressure while minimizing energy exposure to the skull. By reducing cranial heating risks and ensuring adequate energy reaches the focal point, phased arrays contribute to safer and more effective neuromodulation (Smith *et al.*, 2022). However, phased array transducers can generate side or grating lobes, leading to off-target stimulation. This is a significant challenge in ensuring precise neuromodulation. Besides, the design, fabrication, and integration of phased array transducers and their electronics are complex and costly. The large size and mass of phased array transducers, along with thick cables, strongly limit their application in small animals and restrict the free movement of subjects during experiments. (Kyriakou *et al.*, 2014)The bulky design of phased array transducers requires the use of anesthesia or physical restraint in ultrasound therapy experiments on small animals. Unfortunately, anesthesia alters normal brain activity, which can significantly bias the results of neuromodulation studies by disrupting natural neural responses(Zarhin *et al.*, 2022). This interference poses a challenge as the altered physiological state under anesthesia does not accurately represent normal brain function. In this respect, using single-element transducers for neuromodulation in mice offers several advantages, particularly in portability, precision, cost, and safety(He *et al.*, 2023; Hu *et al.*, 2023). One study (Hou *et al.*, 2022) developed a 1 MHz concave single-element transducer with a radius of curvature of 5 mm and an aperture diameter of 7.5 mm for deep brain stimulation, based on simulation results, and achieved precise and effective ultrasonic

neuromodulation. The study in (Lee *et al.*, 2018)developed a wearable t-FUS transducer (with a diameter of 16 mm, a center frequency of 600 kHz, and a weight of 6 grams) to stimulate motor cortical areas in awake rats. Another study (Meng *et al.*, 2024) designed and fabricated a 3.8 MHz wearable single-element transducer that weighs about Another study (Meng *et al.*, 2024) designed and fabricated a 3.8 MHz wearable single-element transducer that weighs about 2 gramsg, for freely moving mice to stimulate the deep brain hypothalamus. 2 grams, for freely moving mice to stimulate the deep brain hypothalamus. The single-element transducer has gained popularity in small animal studies due to its ease of handling and low manufacturing cost, making it an accessible and practical option for preclinical neuromodulation research.

The majority of existing studies have concentrated on superficial or cortical brain regions (Airan and Butts Pauly, 2018; King *et al.*, 2014; Legon *et al.*, 2018b), where ultrasound energy traverses relatively short paths through the skull and encounters minimal attenuation. These shallow targets allow for simpler acoustic coupling, less sensitivity to skull heterogeneity, and more predictable beam propagation. In contrast, deep brain targets pose significant technical challenges due to increased propagation distance, complex refraction and reflection at the skull interfaces, and substantial absorption and phase aberration through heterogeneous media. Despite the growing interest in t-FUS for neuromodulation, an optimized single-element transducer design for targeting deep brain regions, such as the hypothalamus, has not yet been developed. Designing such a transducer involves addressing multiple parameters, including frequency, radius of curvature, aperture diameter, skull-induced distortions, and other FUS parameters (Labib *et al.*, 2024)Designing such a transducer involves addressing multiple parameters, including frequency, radius of curvature, aperture diameter, skull-induced distortions, and other FUS parameters (Labib *et al.*, 2024). (Labib *et al.*, 2024). These factors collectively determine the effectiveness and precision of targeting deep brain structures. The hypothalamus, a critical deep brain region (see Figure 1), plays a central role in regulating essential physiological and behavioral functions, such as the endocrine system, body temperature, blood pressure, hunger, thirst, mood, and sleep (Saper and Lowell, 2014). Stimulating the hypothalamus may affect food intake behavior (Meng *et al.*, 2024), aging (Pang *et al.*, 2021), and thermoregulation of the body (Pang *et al.*, 2022). However, while these findings are compelling, comprehensive long-term studies are needed to fully understand the sustained effects of hypothalamic stimulation on these complex functions.

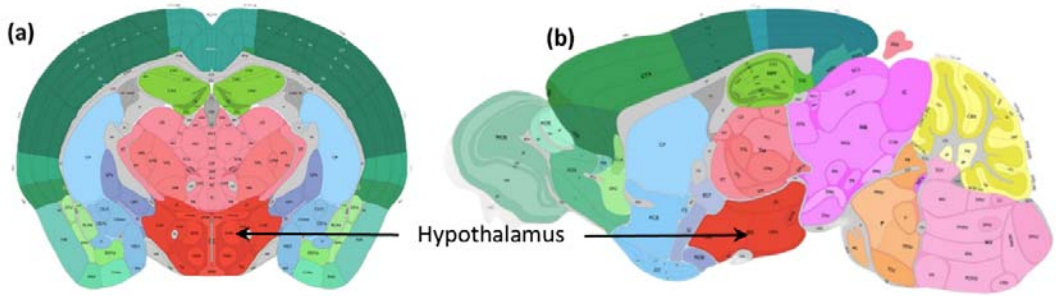

Figure 1. Location of the hypothalamus in the mouse brain in (a) coronal view and (b) sagittal view. The hypothalamus, a critical deep brain structure, is situated near the lower skull bone and plays a central role in regulating essential physiological and behavioral functions, including the endocrine system, body temperature, hunger, thirst, mood, and sleep.

Conventionally, single-element transducers are designed using an empirical approach, highly relying on literature or prior experiences. However, mouse skull anatomy introduces unique acoustic challenges, particularly in transmitting energy through the upper skull to reach deeper regions

adjacent to the lower skull due to skull-induced attenuation, reflection, and acoustic aberration. This study aims to develop an optimization framework that integrates acoustic simulations, machine learning-based surrogate modeling, and an evolutionary algorithm to optimize single-element transducer design parameters for deep brain targeting in mice, with a focus on the hypothalamus. In the simulation phase, the transducer design parameters: frequency, ROC, and f-number are systematically varied. Later, a Random Forest (RF) model is trained on the acoustic simulations to predict five performance metrics: focal length, focal shape, maximum pressure, location of peak pressure, and side lobe suppression. This surrogate model is integrated with the NSGA-II multi-objective optimization algorithm to efficiently identify high-performing transducer design parameters.

2. Materials and methods

2.1. A mouse head model

The first step in designing an effective transcranial ultrasound transducer is to select a realistic model that accurately reflects the geometric and material properties of the mouse head. In this study, mouse head CT images obtained from the IMAIOS Vet-Anatomy website (Hoa, 2018) were chosen to aid in modeling mouse heads. These images provide a detailed visualization of the structural layout of the mouse head, facilitating the numerical optimization of ultrasound energy delivery in transcranial focused ultrasound (t-FUS) research. As shown in Figure 2, this study opted to model the mouse head as a 2D medium instead of a 3D medium. The main reason for this decision is that the transducer developed in this study is a spherical single-element transducer, whose geometric symmetry ensures that sound distribution in the coronal and sagittal planes together can provide adequate information for evaluating the transducer's performance. Additionally, 2D simulations are computationally more efficient than their 3D counterparts, facilitating the transducer parameter optimization process.

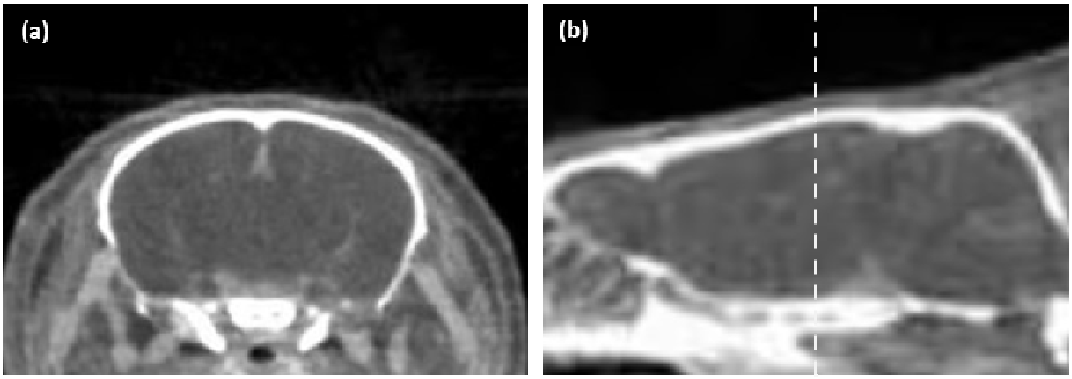

Figure 2. CT images of the mouse brain in the (a) coronal and (b) sagittal perspectives. The coronal view highlights the bilateral symmetry of the brain and the relative positions of subcortical areas; the sagittal view provides insight into the depth and proximity of deep brain regions, such as the hypothalamus, to the skull bones. The dashed line in (b) shows the position of (a) in the sagittal plane. Images are adapted from IMAIOS Vet-Anatomy (Hoa, 2018).

Based on the mouse head model in Figure 2, the medium is further divided into three regions—water, skull, and soft tissue—as depicted in Figure 3, according to their distinct mass densities. Please note that the mouse brain and skin are modeled as the same medium, referred to as soft tissue,

because of their negligible differences in acoustic parameters. Assuming each region is homogeneous, the material properties listed in Table 1 are assigned to the corresponding regions, forming a simplified model of the mouse brain as shown in Figure 3. In this model, the average skull thickness of the mouse is approximately 0.3 mm (Ghanbari *et al.*, 2019; Macmanus, 2023). The power law absorption exponent is set to 1.08 (Treeby *et al.*, 2012) as a scalar input since k-Wave only allows for a single value for the entire model.

In addition, the relative position of the single-element transducer in relation to the mouse brain and the transducer's primary geometries are also demonstrated in Figure 3. For a single-element spherical transducer, the primary geometric properties include its radius of curvature (ROC) and aperture diameter.

Table 1. Material properties adopted in simulating the transcranial ultrasound energy delivery: speed of sound ( ), mass density ( ), power law absorption prefactor ( ), power law absorption coefficient (*y*), and nonlinearity parameter (*B/A*).

	(m/s)	(kg/m^3)	(dB/MHz^y cm)	*y*	*B/A*
Water (Pantea *et al.*, 2013)	1500	1000	0.0022	1.08	3.5
Skull (Liang *et al.*, 2019; Jiménez-Gambín *et al.*, 2022)	2425	1933	8.8400	1.08	8.0
Soft tissue (Jiménez-Gambín *et al.*, 2022)	1540	1040	0.4160	1.08	6.5

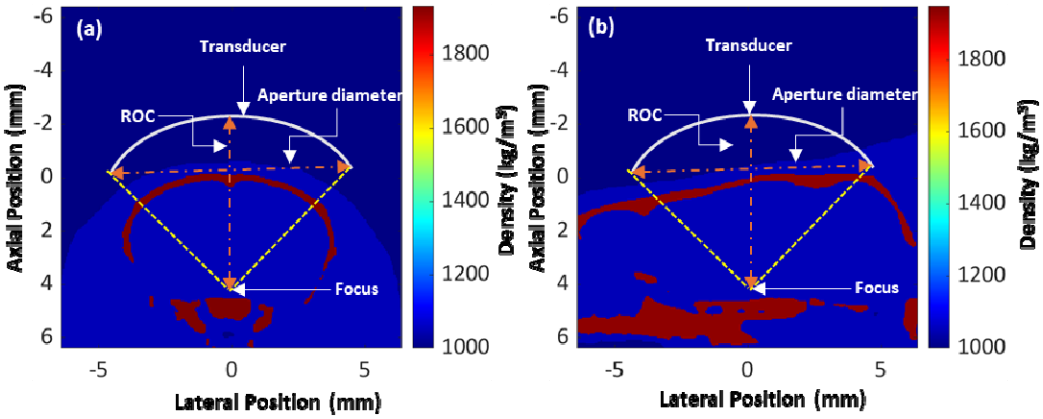

Figure 3. (a) Coronal and (b) sagittal views of the mouse brain model. This model highlights three distinct regions: water (low density), skull (high density), and soft tissue (intermediate density), which provides a comprehensive representation of the anatomical and acoustic properties of the mouse head. This model also illustrates the transducer's relative position in relation to the mouse brain and its primary geometries: ROC and aperture diameter.

2.2. *k*-Wave simulation

To date, various simulation methods, including semi-analytical methods (e.g., ray tracing and transfer function methods) and numerical methods (e.g., finite differences and k-space), have been adopted for wave propagation simulation (Angla *et al.*, 2023). In this study, we adopted k-Wave, a widely used open-source MATLAB toolbox for acoustic simulation. k-Wave is built on a k-space pseudospectral method, which provides an efficient way to model the propagation of sound with high accuracy (Treeby and Cox, 2010). It is specifically designed for solving acoustic wave equations in complex, homogeneous, or heterogeneous media using a time domain approach (Treeby and Cox

2010). Moreover, k-Wave supports modeling of sharp discontinuities, such as the interface between bone and soft tissue encountered in this study, which is critical for accurately predicting how waves propagate through different layers of tissue (Treeby *et al.*, 2012).

In this study, we simulated the propagation of ultrasound waves originating from a single-element spherical transducer as they traveled through an inhomogeneous medium (water, bone, and soft tissue) and ultimately focused on a deep brain location. This simulation models the behavior of ultrasound waves as they pass through an inhomogeneous medium while accounting for key material factors such as the speed of sound, mass density, and nonlinearity. The main purpose of the simulation is to understand how the primary characteristics of ultrasound beams are affected by the transducer's operating frequency and geometry.

The key parameters and operations of the simulation in this study are described below. The grid size was set to 512 × 512 grid points (12.8 mm × 12.8 mm) with a spatial resolution of 0.025 mm. The medium was assigned the material properties listed in Table 1. A spherical single-element transducer, functioning like an arc-shaped transducer in 2D, was positioned outside the mouse head as shown in Figure 3. While the ROC and aperture diameter varied throughout the study, the transducer's position also changed to target the same deep brain region. For all the studied cases, a Gaussian-windowed tone burst signal with 10 cycles was emitted from the transducer. The k-Wave function 'kspaceFirstOrder2D' was used to simulate wave propagation in the time domain. At each time step, the pressure and particle velocity fields were calculated. A 2D grid of the same size as the simulation area was used as the sensor to store the simulated acoustic pressure, intensity, and particle velocity for further analysis.

To achieve deep-brain stimulation, the geometric focus (the center of curvature) of each transducer was set to a deep-seated structure located at (0 mm, 4 mm) in the lateral and axial directions, as shown in Figure 3. This focal arrangement was selected to ensure anatomical relevance in deep-brain murine neuromodulation studies, in which brain regions such as the hypothalamus and brain stem are of interest. The simulated acoustic fields were presented using the root-mean-square pressure (rms pressure, P_{RMS}) and intensity (I_{RMS}). P_{RMS} was obtained from the time-varying pressure distribution, and I_{RMS} was calculated using the following relation:

$$I_{RMS} = \frac{P_{RMS}^2}{\rho c} \tag{1}$$

The computed intensity field was first normalized against the maximum value of the field and then converted to decibel scale (dB) to facilitate visual interpretation and comparative analysis. This approach enabled the identification of high-intensity focal regions and evaluation of off-target energy exposure, including energy deposition within the skull bones and adjacent tissues.

2.3. Performance evaluation for transducer designs

To assess the performance of transducer designs, we identified the key parameters of the acoustic field for each design based on conventional standards for acoustic field evaluation. The following parameters are considered in this study for evaluating the generated ultrasound field.

(i) *Focal length*. The focal region's dimensions, particularly its length, are critical in assessing the precision and spatial confinement of the focused ultrasound beam. In concave-shaped transducers, the focal length is generally larger than the focal width due to their natural beam convergence properties (Murphy *et al.*, 2025). Therefore, the focal length is used as one of the key parameters for evaluating the performance of a transducer design. In this study, focal length is measured as the axial length of the -3 dB focal region of the acoustic intensity field. In both coronal and sagittal planes, the intensity fields were evaluated using the decibel scale, computed with reference to the maximum acoustic intensity observed in the coronal and

sagittal planes. Figure 4(a)-(c) illustrates the method of determining the focal length under different focal shapes. Focal length was expressed in millimeters, with shorter focal lengths preferred due to their ability to provide more precise targeting.

(ii) *Focal shape*. Since the goal of this study is to develop single-element transducers for deep brain stimulation, we chose the hypothalamus, which is located approximately 1.5 mm to 2 mm above the lower skull bone (Wang *et al.*, 2020), as the targeted brain region in our designs. Because this target is closer to the lower skull, the focal shape is strongly affected by the sound reflections from the lower skull: The interference of the incident and reflected sound leads to unconventional -3 dB focal shapes, as shown in Figure 4(a)-(c). To facilitate the generation of a numerical transducer quality matrix, different focal shapes were assigned categorical scores to reflect the irregularity of the focal region: a score of 2 indicated a regular focal region, 1 for a moderately distorted focal region, and 0 for a highly distorted focal region. Thus, a larger score indicates a higher ability of a transducer design to deliver ultrasound energy precisely to the hypothalamus while minimizing off-target stimulation.

(iii) *Maximum pressure at the focal region*. The maximum value of the root-mean-square (RMS) pressure at the transducer's focal region provides a quantitative measure of the localized energy delivered to the target region. It reflects the effectiveness of energy coupling through the skull and directly correlates with the therapeutic potential of the transducer. Therefore, in this study, the RMS pressure at the focus was measured to evaluate the transducer’s ability to deliver acoustic energy to the intended target. The pressure was quantified in Pascals (Pa) with higher values indicating greater energy deposition at the focal region.

(iv) *Location of the maximum pressure of the field*. The position of the maximum pressure of the acoustic field in each plane was identified to ensure precise targeting of the desired brain structures while minimizing the risk of excessive energy deposition outside the targeted region. As shown in Figure 4(d)-(f), this criterion also employs categorical scoring: a score of 2 is assigned if the maximum pressure is located in the focal region, 1 if at the lower skull bone, and 0 if at the upper skull bone.

(v) *Sidelobe level*. The amplitude of the sidelobes is considered a key criterion for assessing off-target energy distribution. Sidelobe level was evaluated as a binary variable, with a score of 1 indicating the absence of sidelobes above −10 dB and a score of 0 indicating their presence. This metric helps ensure that the acoustic energy remains concentrated at the target and does not spread to unintended regions. Figure 4(g)-(h) depicts this evaluation criterion.

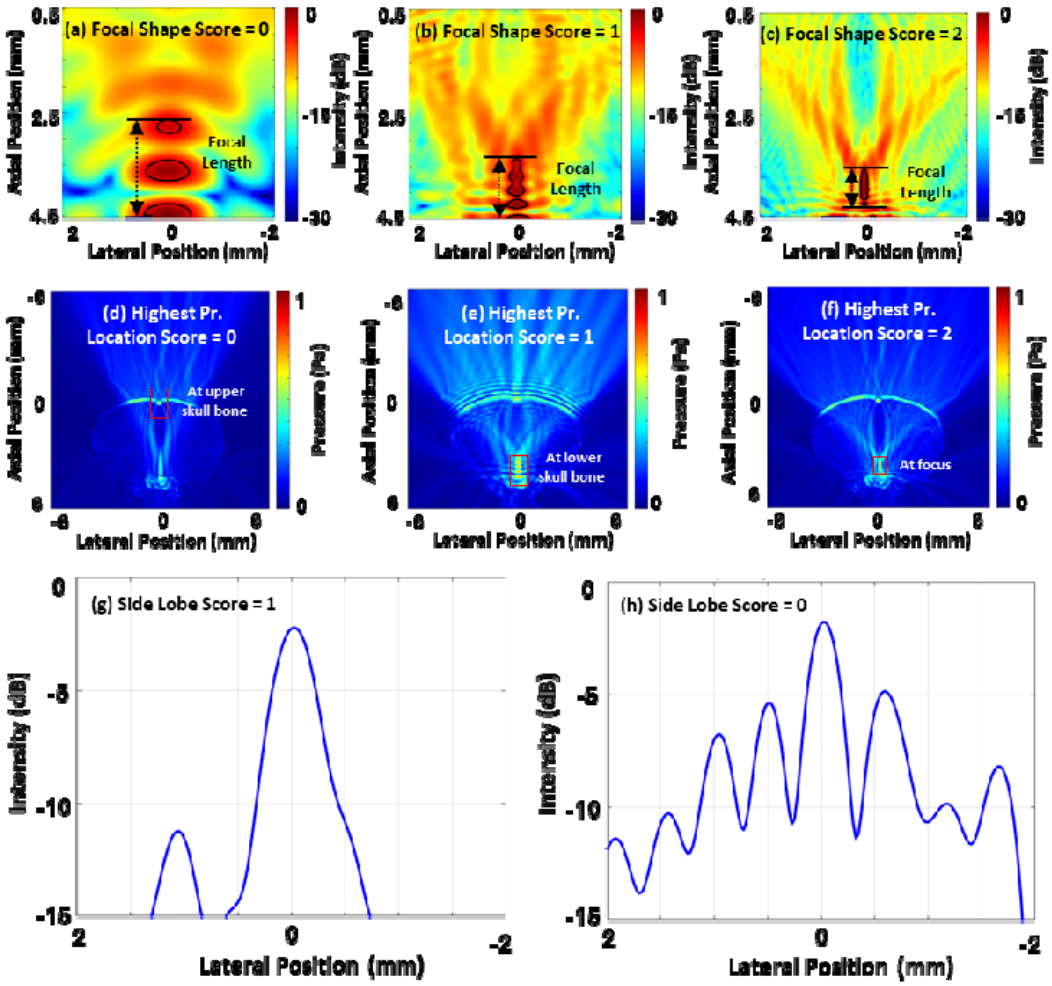

Figure 4. Illustration of the parameters used for the transducer performance evaluation. (a), (b), and (c) illustrate the determination of focal length for three cases of focal shape score: 0 for highly distorted focal shape, 1 for moderately distorted shape, and 2 for uniform shape. (d), (e) and (f) demonstrate the scoring criteria for the location of the maximum pressure of the entire acoustic field: 0, 1, and 2 corresponding to the locations at the upper skull, the lower skull, and the target focal zone, respectively. (g) and (h) present the evaluation of sidelobe suppression, indicating the presence of sidelobes below and above -10dB.

2.4. Effect of transducer's working frequency on its performance

An essential consideration in developing a t-FUS transducer is selecting its working frequency, as it significantly influences the characteristics of ultrasound wave propagation and subsequent energy delivery. Generally, the frequency of ultrasound waves directly impacts the targeting precision, penetration depth, and energy deposition into targeted tissues. Higher frequencies yield shorter wavelengths, enabling sharply defined focal spots, thus facilitating more precise tissue targeting. However, higher frequencies experience significant attenuation when passing through a dense medium, such as the skull, resulting in notable energy loss and localized heating. The energy attenuation greatly reduces the penetration depth of high-frequency transducers. The localized heating can pose risks of tissue damage. Conversely, lower-frequency ultrasound waves possess longer wavelengths, which allows them to penetrate deeper into brain tissues with reduced attenuation, but with decreased spatial resolution. The broader focal zones associated with lower frequencies may inadvertently stimulate regions beyond the intended targets, reducing neuromodulation precision. Additionally, low-frequency waves tend to create standing-wave patterns

within the cranial cavity, complicating the accurate delivery and distribution of ultrasound energy (Samoudi *et al.*, 2019b).

In practice, frequency selection can also influence the size of the transducer. Lower-frequency transducers must employ larger piezoelectric elements to effectively generate and focus the ultrasound beam, resulting in bulky designs. In contrast, higher-frequency transducers can be more compact, using smaller piezoelectric elements due to shorter acoustic wavelengths. Therefore, optimizing frequency involves balancing precision, penetration depth, tissue safety, and device size to meet specific neuromodulation objectives.

According to the literature, various frequencies have been utilized to study transcranial ultrasound neuromodulation in rodent models. For example, 3.8 MHz (Meng *et al.*, 2024) and 3.74 Hz (Huang *et al.*, 2022) single-element transducers have been used to stimulate the mouse hypothalamus. In another study (Hu *et al.*, 2022), single-element transducers of 1.5 MHz, 3.0 MHz, and 6.0 MHz have been used in blood-brain barrier opening for preclinical research in mice. Single-element 1.0 MHz transducers with varying transducer geometry (ROC of 5 mm, and aperture diameters of 5 mm and 7.5 mm) successfully stimulated the primary motor cortex of mice (Hou *et al.*, 2022). While a wide range of transducer frequencies has been used in previous studies, the selections are often heuristic rather than the result of systematic optimization. Therefore, this study aims to determine the optimized working frequencies of transducers by investigating the effects of various frequencies on deep brain neuromodulation in mice. Specifically, we varied the transducer frequency from 1.0 MHz to 6.0 MHz in a 1 MHz increment to assess its impact on the mouse brain and the focal region.

2.5. Effect of transducer's geometry on its performance

Another important consideration in designing an ultrasound transducer is its geometry, which fundamentally shapes the acoustic field's properties, governing focal sharpness, beam width, pressure amplification, and off-target energy deposition. A single-element focused ultrasound transducer has two critical geometric parameters: the radius of curvature (ROC) and the aperture diameter. Typically, the relationship between the ROC and aperture diameter can be expressed in terms of the f-number, which is defined as the ratio of ROC to aperture diameter. This dimensionless parameter is a key descriptor of the transducer's geometric focusing characteristics and is used to evaluate how transducer geometry influences the resulting acoustic field distribution. Specifically, lower f-numbers generate convergent beams with higher energy amplification, while higher f-numbers yield broader, less intense beams with greater depth of field (Murphy *et al.*, 2025). Geometric design also inherently interacts with Fresnel zone behavior. Lower f-number transducers tend to create smaller effective Fresnel zones, enhancing lateral resolution but at the expense of increased sensitivity to phase aberrations. Larger f-numbers, on the other hand, extend the Fresnel zones, distributing energy over wider areas and reducing the system's ability to discriminate fine spatial features.

In this study, we investigate how the interaction between acoustic energy and the skull and soft tissues affects the transducer's acoustic field performance when transducers with varying ROCs (5-7 mm) and f-numbers (0.58-1.0) are positioned over the mouse head. The focus remains consistently on a targeted deep brain region, and as the transducer's ROC changes, the distance between the transducers and the mouse head is also adjusted accordingly.

2.6 Optimization method for designing transducers

Built upon the considerations discussed in sections 2.4 and 2.5, we defined the design parameter space as follows: 1-6 MHz for the working frequency, 5-7 mm for the ROC, and 0.58-1.0 for the f-

number, aiming to generate the best design of a single-element transducer for deep-brain stimulation in mice. The continuous nature of the design parameter space implies an infinite number of feasible transducer designs. Conducting full acoustic simulations for every possible combination would be computationally expensive. Therefore, we chose to use an optimization method to facilitate the transducer design process, reducing computational cost while maintaining design quality.

The optimization method employed in this study was a surrogate-based approach. This approach belongs to the class of data-driven evolutionary optimization algorithms, where a machine learning model (the surrogate) is trained to approximate the computationally expensive objective function. The key advantage of this surrogate-based strategy lies in its ability to predict and optimize complex system behavior with significantly reduced computational effort, while still capturing the intricate trade-offs between multiple performance metrics. In this approach, a Random Forest (RF) regression model was employed as the surrogate predictor to approximate the performance of the transducer designs across the multidimensional parameter space. RF was selected due to its proven capability in modeling complex, nonlinear input-output relationships, its inherent resistance to overfitting when handling moderate-sized datasets, and its robustness against multicollinearity among input features (Khan *et al.*, 2021; Garg *et al.*, 2023). The surrogate was then coupled with an evolutionary search algorithm to identify transducer designs that maximize the desired acoustic performance criteria. In this study, the Non-dominated Sorting Genetic Algorithm II (NSGA-II), a well-established evolutionary algorithm specifically designed for multi-objective problems characterized by discrete decision variables, nonlinearity, and conflicting performance trade-offs (Chen *et al.*, 2022; Liu *et al.*, 2024), was used for identifying the optimized transducer designs. NSGA-II was obtained from the Distributed Evolutionary Algorithms in Python (DEAP), an open-source Python library for evolutionary computation.

The implementation procedures of the surrogate-based transducer design optimization method are described below:

(i) *Define initial transducer design parameters*. To systematically optimize the transducer geometry and frequency for the targeted deep-brain ultrasound delivery, the design process starts with selecting initial transducer parameters. In this study, we selected three design values for ROC (5, 6, and 7 mm), four values for f-number (0.58, 0.67, 0.85, and 1.0), and six values for frequency (1, 2, 3, 4, 5, and 6 MHz), resulting in 72 sets of design parameters

(ii) *Simulate the acoustic field using k-Wave*. Following the method described in Section 2.2, full-wave simulations were performed in both coronal and sagittal planes on 72 sets of design parameters, resulting in 144 acoustic intensity images and 144 RMS pressure images.

(iii) *Identify the parameters used for evaluating transducer performance*. For each of the 72 cases, two acoustic intensity images (obtained from the coronal and sagittal planes, respectively) and two RMS pressure images were assessed using the evaluation parameters defined in Section 2.3. Among these parameters, focal length and the maximum pressure at the focal region are continuous, and the rest of the parameters are categorical. The evaluation criteria were strategically chosen to prioritize focal precision, acoustic field quality, and biological safety, ensuring that optimized designs not only precisely deliver energy but also minimize the risk of off-target tissue exposure. By the end of this step, 72 datasets were generated, each including three transducer properties (f-number, ROC, and frequency) and ten transducer performance evaluation parameters (five for the coronal plane and five for the sagittal plane).

(iv) *Generate and evaluate the surrogate model*. Based on the results of the last step, we compiled a database of 72 datasets, each comprising three input variables (transducer design parameters) and ten output variables (transducer performance parameters that represent the

combined performance across both planes). To construct the predictive surrogate model, RF algorithms were employed for both regression and classification tasks based on the nature of the output variables. The complete dataset was partitioned so that 80% of the data was used for training, and the remaining 20% was reserved for evaluating the algorithm's performance. For each continuous output variable, such as the focal length and maximum pressure at the focal region, separate RF regression models were trained using the same set of three independent input variables: f-number, ROC, and frequency. In parallel, RF classification models were independently trained for each categorical performance metric, including the location of the maximum pressure score, focus shape score, and side lobe suppression score. This modular modeling strategy ensured that the surrogate system could accurately map the design input. The training process was carried out using custom Python code in a Google Colab notebook, leveraging the open-source library 'scikit-learn' for model development. The model was evaluated with the reserved 20% of the data, and the evaluation demonstrated high predictive accuracy, as shown in Table 2. The coefficient of determination (R^2) is a fundamental metric used to assess the performance of RF regression and classification models. It reflects how well the model explains the variability in the target variable. A value of 1 denotes a perfect fit, whereas a value of 0 implies that the model fails to account for any of the variability. This strong correlation confirms that the surrogate captures the dominant underlying physics governing the acoustic field responses, thus providing a computationally efficient and reliable foundation for subsequent optimization.

(v) *Perform design optimization using an evolutionary algorithm*. For design optimization, NSGA-II was coupled with the trained RF surrogate model to efficiently navigate the design space, eliminating the need for additional acoustic-field simulations. The evolutionary parameters were empirically tuned to ensure an effective balance between exploration and exploitation, using a population size of 100, a crossover probability of 0.6, and a mutation probability of 0.3. Gaussian mutation was applied with a mean of zero and a standard deviation of 0.1 to introduce variability while maintaining stability in the search process. The optimization was run for 60 generations, yielding a set of Pareto-optimal transducer designs that maximize or minimize the defined output parameters while adhering to physical design constraints.

Table 2. The coefficients of determination (R^2) of the Random Forest (RF) regressors and classifiers.

	Performance evaluation criteria	Data type	RF model	R^2
Coronal plane	Focal length	Continuous	Regressor	0.865
	Focal shape	Categorical	Classifier	0.800
	Maximum pressure at the focal region	Continuous	Regressor	0.895
	Location of the maximum pressure of the field	Categorical	Classifier	0.867
	Side lobe	Categorical	Classifier	0.867
Sagittal plane	Focal length	Continuous	Regressor	0.801
	Focal shape	Categorical	Classifier	0.800
	Maximum pressure at the focal region	Continuous	Regressor	0.901
	Location of the maximum pressure of the field	Categorical	Classifier	0.733
	Side lobe	Categorical	Classifier	0.867

2.7 Comparison of the optimized design with the existing transducers

To verify the performance of the single-element focused ultrasound transducers optimally designed in this study, we compared the acoustic field of our transducer to that of the transducers reported in the literature (Hou *et al.*, 2022; Hu *et al.*, 2022) with similar functions. The working frequency and geometric properties of these transducers were used as reported in the literature, while the focal position was set the same as our transducer. The acoustic field of the selected transducers was computed using the same method as in our simulation.

3. Results

3.1. Optimized design of the transducer

This study employed a machine learning-guided multi-objective optimization strategy to identify an optimal transducer design that can precisely target deep brain structures. Utilizing the framework outlined in Section 2.6, the optimal design parameters were determined to be a f-number of 0.57, ROC of 5.75 mm, and a frequency of 6.0 MHz. Figure 6 presents the acoustic intensity field simulated using the best-performing transducer parameters, as predicted by the optimization framework. The simulation results confirm that this design yields a highly localized and nearly symmetric focal region targeting the hypothalamus region of the mouse brain, with minimal side lobe artifacts and effective energy confinement away from skull interfaces, as illustrated in Figure 5. As discussed earlier, the decibel scale acoustic intensity was computed with reference to the maximum intensity observed in either the coronal or sagittal plane for each design to more accurately approximate the three-dimensional acoustic field. Notably, in Figure 5(b), no -3 dB focal area was visible, indicating a highly focused and spatially restricted energy distribution in the sagittal plane. In other words, if the 3D focal region is an ellipsoid, its axis in the coronal plane will be much larger than its axis in the sagittal plane, making it a very flat ellipsoid.

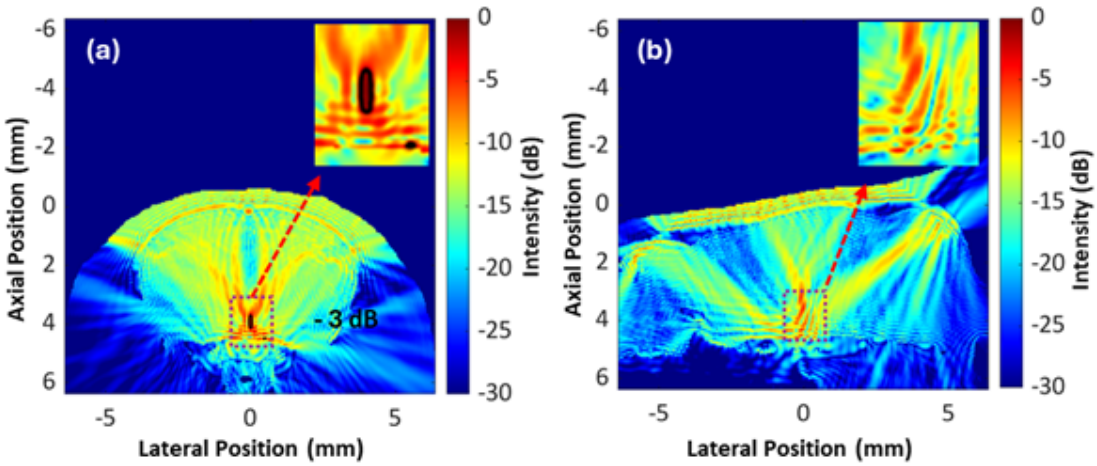

Figure 5. (a) Coronal and (b) sagittal views of the acoustic intensity field of the transducer design optimized by a machine learning-driven process.

To assess the performance of the optimization method in this study, a comparison between the predicted and simulated performance metrics is summarized in Table 3. Except for the maximum pressure at the focal region, all other predicted performance evaluation metrics closely matched the simulation results. The deviation in maximum pressure between predicted and simulated values was 8% in the coronal plane and 4.5% in the sagittal plane. This comparison further underscores the

effectiveness of machine learning-guided optimization in transducer design for transcranial neuromodulation.

Table 3. Comparison of the optimized transducer's predicted and simulated performance.

	Performance evaluation criteria	Predicted Value	Simulated Value
Coronal plane	Focal length	0.45 mm	0.45 mm
	Focal shape	2	2
	Maximum pressure at the focal region	0.80 Pa	0.87 Pa
	Location of the maximum pressure of the field	2	2
	Side lobe	1	1
Sagittal plane	Focal length	0 mm	0 mm
	Focal shape	0	0
	Maximum pressure at the focal region	0.44 Pa	0.42 Pa
	Location of the maximum pressure of the field	0	0
	Side lobe	1	1

3.2. Comparison of the optimized transducer design and those reported in the literature

To assess the performance of the single-element focused ultrasound transducers optimally designed in this study, we compared the acoustic field of the transducer optimally designed in this study with that of several transducers of similar function reported in the literature. The transducers to compare include 1 MHz transducers with a fixed f-number of 1 and ROCs of 5 and 7.5, which were identified to be optimal within their design space in (Hou *et al.*, 2022) and three transducers with a 10 mm ROC and f-number of 0.77 across multiple frequencies (1.5 MHz, 3.0 MHz, and 6.0 MHz), targeting generalized neuromodulation applications (Hu *et al.*, 2022).

To ensure a consistent benchmark, we replicated the acoustic field of these five designs, and compared their -3 dB acoustic intensity fields with that of our machine learning-guided optimized transducer. As illustrated in Figure 6, the optimized design outperforms the literature-reported designs. It demonstrates superior energy localization, with a tighter and more confined focal zone (0.125 mm laterally and 0.425 mm axially) key attributes for targeting deep brain regions such as the hypothalamus. In the sagittal plane, a -3 dB focal area was not exhibited in most cases; therefore, the comparison is only shown in the coronal plane.

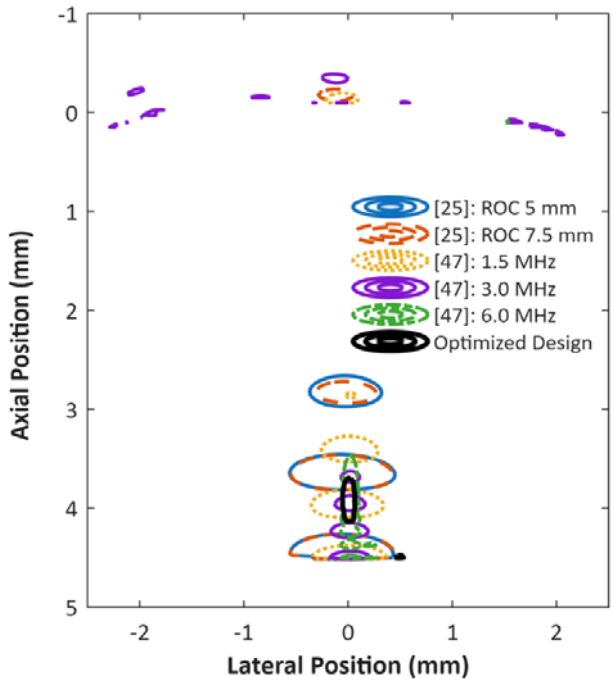

Figure 6. Comparison of the -3 dB acoustic intensity field in the coronal plane of the optimized transducer design in this study and the similar transducer designs reported in the literature.

4. Discussion

To show the contribution of three transducer design parameters (f-number, ROC, and frequency) to the performance metrics of the transducer, a feature importance analysis was conducted on the trained RF model. Feature importance in random forests is derived from the mean decrease in impurity (MDI), where the importance of a feature is computed based on how much it reduces the weighted variance (for regression) or Gini impurity (for classification) across all decision trees in the ensemble. Higher importance values indicate that a feature contributes more significantly to the model's predictive performance.

Each of the ten output parameters was associated with an independent RF model. Feature importance was extracted from all ten models to provide a comprehensive understanding of how each design parameter influences different performance outcomes, as in Figure 7. Detailed analysis of the effect of transducer design parameters on each performance evaluation criterion is discussed later in this section.

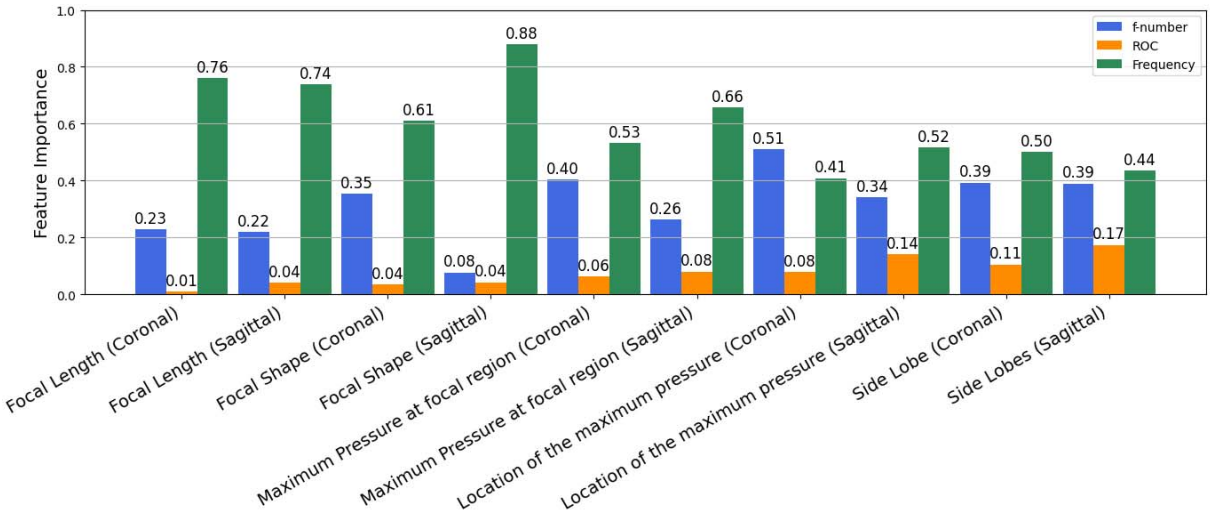

Figure 7. A consolidated bar chart showing the relative importance of three transducer design parameters on the five transducer performance parameters in each imaging plane in the surrogate model

4.1. The effect of transducer design parameters on focal length

Focal length, the axial extent over which the acoustic intensity remains above a threshold (-3 dB), directly influences spatial selectivity in ultrasound neuromodulation. Shorter focal lengths are preferred as they allow localized stimulation of neural targets while minimizing unintended exposure to adjacent structures. In this study, focal length was analyzed across 144 acoustic intensity fields for both coronal and sagittal planes. As shown in Figure 7, frequency strongly governs the focal length, with feature importance scores of 0.76 for coronal plane, and 0.74 for sagittal plane. This result reflects the well-established inverse relationship between frequency and wavelength. The f-number also contributes modestly, 0.23 and 0.22 in coronal and sagittal planes, respectively. The ROC, by contrast, has a negligible effect (<0.05), suggesting that for the focal length range examined.

Since the frequency has a stronger impact on the focal length compared to the other two design parameters, we further analyze the effect of frequency on the focal length, as shown in Figure 8. As the frequency increased, the focal length decreased. However, at the sagittal plane this trend was partially offset by increased beam distortion and acoustic attenuation through the skull due to the asymmetry of cranial anatomy. As previously noted, the acoustic field in the sagittal plane, for certain design cases, especially those at higher frequencies, failed to exhibit a well-defined -3 dB focal region, indicating challenges in maintaining focus under such conditions. These plots highlight the frequency-dependent spatial confinement of the acoustic field, suggesting the necessity of higher frequencies for a smaller focal region or a more focused sound field.

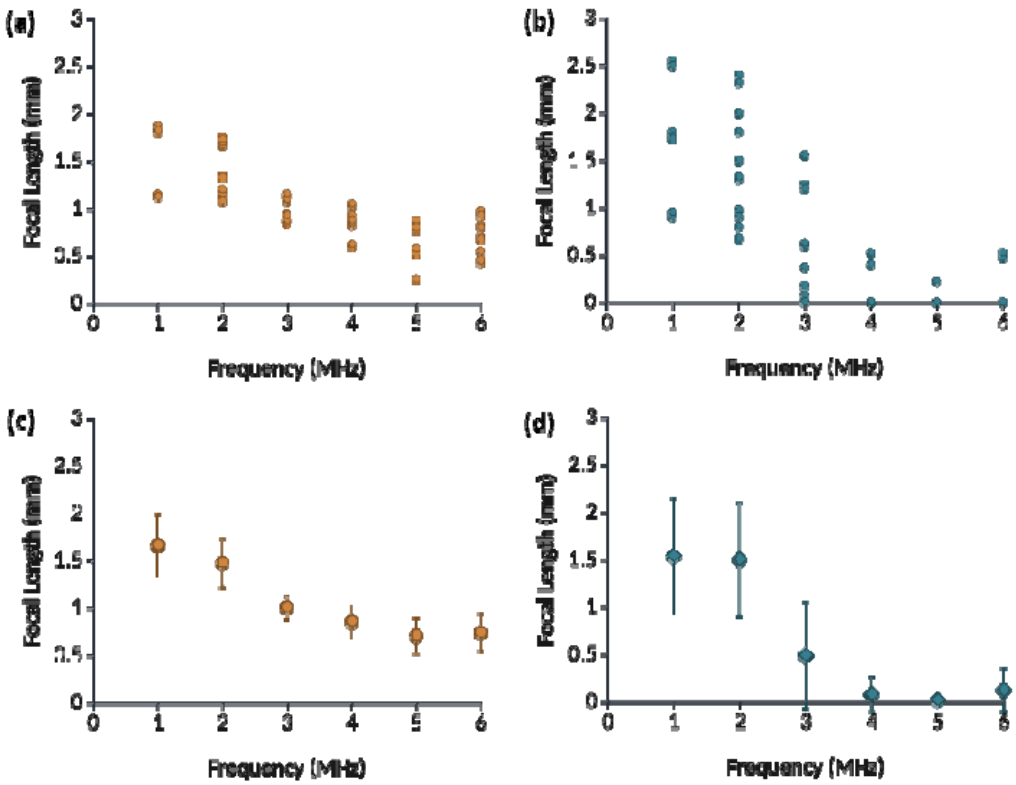

Figure 8. Effect of transducer frequency on focal length in both coronal and sagittal planes. (a) and (b) show the distribution of focal lengths from all 72 simulation cases at varying frequencies in the coronal and sagittal planes, respectively. An inverse relationship can be observed between frequency and focal length. (c) and (d) present the corresponding mean focal lengths and their standard deviation, aggregated by frequency. The inverse relationship was clearly confirmed.

4.2. The effect of transducer design parameters on the focal shape

The spatial morphology of the focal region plays a critical role in determining the specificity and efficacy of t-FUS stimulation. A uniform, well-confined focal shape ensures targeted energy deposition and minimizes off-target acoustic exposure, thereby reducing the risk of undesired neural activation or tissue heating. In this study, the focus shape was qualitatively categorized into three levels: highly distorted, distorted, and uniform, based on the symmetry and compactness of the acoustic intensity distribution in both coronal and sagittal planes. The results illustrated in Figure 7 indicate that frequency is the most influential parameter shaping the focal area, with feature importance values of 0.61 in the coronal plane and 0.88 in the sagittal plane. This strong dependence underscores the role of frequency in controlling acoustic wavelength and lateral beam resolution, both of which directly impact the spatial distribution of the focal region. In contrast, f-number shows a moderate effect in the coronal plane (0.35), consistent with its role in determining beam convergence and aperture control. However, its importance drops significantly in the sagittal plane (0.08), suggesting that f-number barely has influence on focal geometry relative to frequency when sound goes through an asymmetric structure such as the skull in the sagittal plane. The ROC exhibits nearly no influence on focal shape in both planes (importance = 0.04), indicating that within the design space explored, ROC does not substantially alter the focal profile when frequency and aperture characteristics are fixed.

These results suggest that focal shape optimization should prioritize tuning of frequency and f-number. A similar trend is also observed in Figure 9. Simulation results illustrated in Figure 9 reveal

that the focus shape is highly dependent on the interaction between frequency and f-number. Designs employing higher frequencies (≥ 4 MHz) and lower f-numbers (0.58–0.67) consistently produced uniform focal zones in the coronal plane, Figure 9(a-c). These parameter combinations facilitate tighter wavefront curvature and reduced diffraction, yielding compact and symmetric focal patterns with minimal beam spreading. In contrast, lower frequencies and higher f-numbers were more prone to generating distorted or elongated focal regions. This is particularly evident in the sagittal plane, where skull asymmetry and increased bone thickness introduce additional acoustic aberrations, further degrading focus integrity.

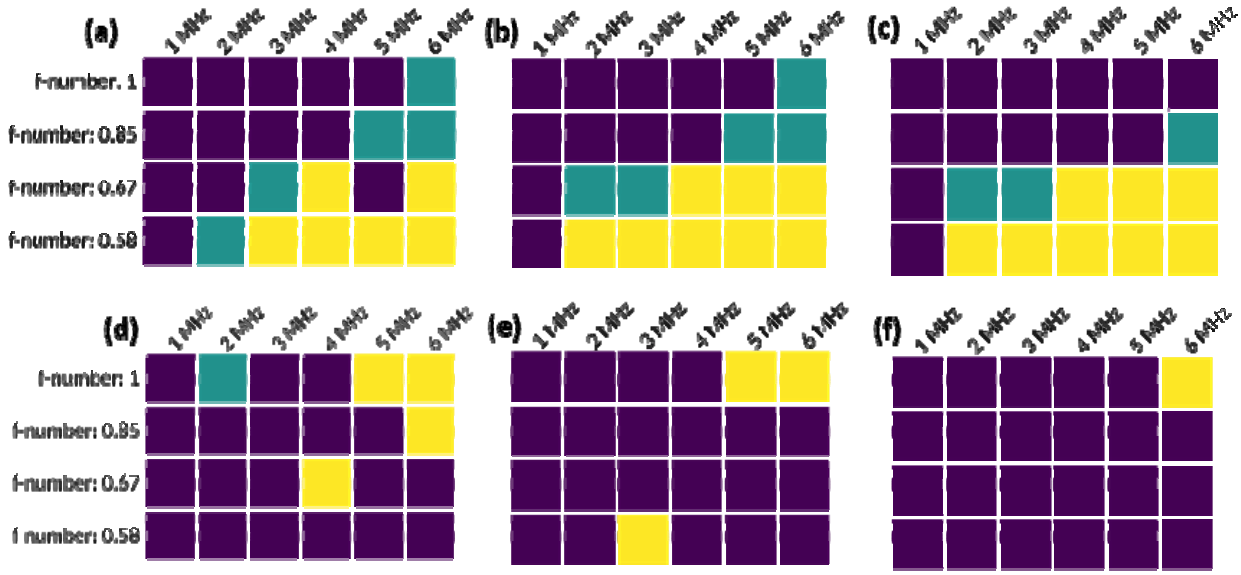

Figure 9. Focal shape distribution across different transducer designs in coronal and sagittal planes. (a-c) show results from the coronal plane for ROC of 5 mm, 6 mm, and 7 mm, respectively; (d-f) present the corresponding data for the sagittal plane. Focal shape is categorized as uniform (yellow), distorted (green), and highly distorted (blue), based on symmetry and beam confinement.

4.3. The effect of transducer design parameters on the maximum pressure at the focal region

The maximum pressure at the focal region is a critical factor influencing the efficacy of t-FUS for neuromodulation, particularly when targeting deep brain regions such as the hypothalamus. The feature importance in Figure 7 reveals that frequency is the most significant contributor in both anatomical planes, with scores of 0.53 in the coronal plane and 0.66 in the sagittal plane. Additionally, the f-number also plays a significant role, with values of 0.40 for the coronal plane and 0.26 for the sagittal plane. In contrast, the ROC demonstrates a minor influence 0.06 in the coronal and 0.08 in the sagittal plane. A detailed description of the effects of transducer design parameters on the maximum pressure at the focal region is shown in Figure 10.

Figure 10 presents the maximum pressure measured at the focal region for various transducer designs. Across all designs, a consistent trend is observed: lower f-numbers yield higher maximum focal pressures. This is because the stronger beam convergence of lower f-number transducers facilitates the concentration of acoustic energy. Additionally, designs with lower frequencies consistently yield higher focal pressures. This is due to the fact that lower-frequency ultrasound experiences reduced absorption and scattering within the skull bone because of its longer wavelength, allowing greater energy to reach deeper targets. In contrast, higher frequencies suffer from pronounced attenuation, especially at the denser cortical bone interfaces, which disproportionately affects the sagittal plane due to its thicker and more inclined skull anatomy.

Comparing the influence of ROC within each plane, the variation in pressure amplitude between 5 mm, 6 mm, and 7 mm ROC is relatively minor, suggesting that focal gain is more sensitive to frequency and f-number than to ROC in the evaluated range. Notably, the pressure magnitudes are slightly higher in the coronal plane than in the sagittal plane across most designs. This discrepancy is attributable to the symmetrical curvature and thinner skull profile in the coronal plane, which reduces acoustic impedance mismatches and enhances transmission efficiency.

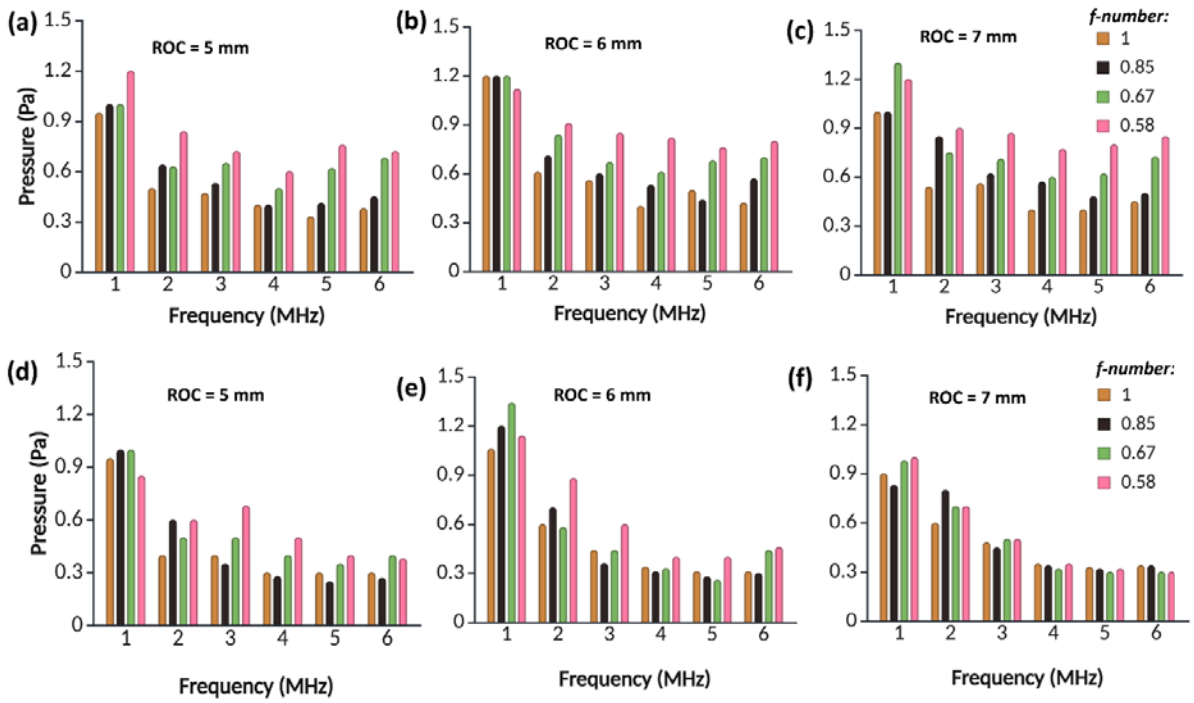

Figure 10. The maximum pressure at the acoustic focus for different transducer designs in coronal and sagittal planes. (a–c) represent coronal plane results for ROC values of 5 mm, 6 mm, and 7 mm, respectively; (d–f) correspond to sagittal plane designs. In each subfigure, the grouped bars represent the maximum focal pressure across different frequencies (1-6 MHz) for f-numbers of 0.58, 0.67, 0.85, and 1.0.

4.4. The effect of transducer design parameters on the location of the maximum pressure in the field

The spatial accuracy of the pressure peak is critical for effective targeting. The feature importance analysis in Figure 7 indicates that both frequency and f-number significantly contribute to determining the location of peak pressure, with varying emphasis between anatomical planes. In the coronal plane, the f-number is the most influential parameter (0.51), followed by frequency (0.41). In the sagittal plane, frequency dominates (0.52) and f-number contributes less (0.34). Both cases suggest that the f-number and frequency together determine the location of the maximum pressure. The ROC has a limited impact (0.08 coronal, 0.14 sagittal), suggesting a secondary role in spatial localization. Overall, optimizing both frequency and f-number is essential for precise control of the pressure maximum across anatomical planes.

Figure 11 illustrates the spatial distribution of the maximum pressure location across different f-numbers and frequencies, as both design parameters have significant effects, depicted in Figure 7. A consistent trend observed across both anatomical planes is that lower f-numbers generally yield more favorable pressure localization, e.g., at the focus marked in yellow. This can be attributed to the higher degree of beam convergence offered by low f-number designs, which enhances focal gain and suppresses off-target pressure artifacts. In both anatomical planes, it was observed that higher

frequencies (4-6 MHz), characterized by shorter wavelengths, tended to concentrate the maximum pressure near the upper skull bone, indicating premature energy deposition. In contrast, lower frequencies with longer wavelengths enabled the pressure peak to shift toward the intended focal region or the lower skull bone. This trend suggests that longer wavelengths are better able to traverse the upper skull layer and deliver acoustic energy more effectively to deeper brain targets.

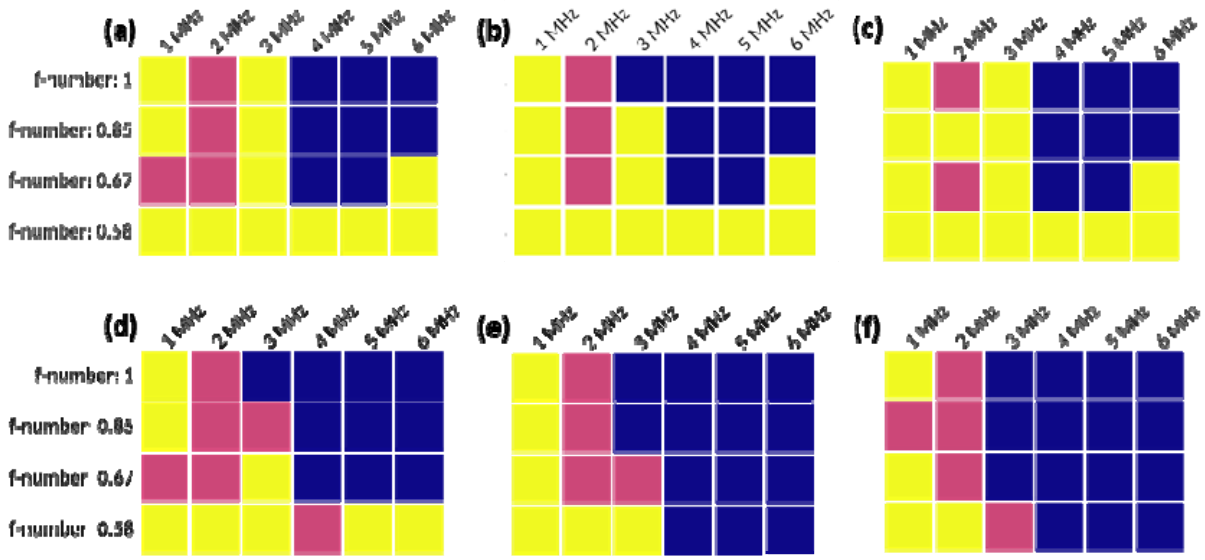

Figure 11. Maximum pressure location distribution across transducer designs in both coronal and sagittal planes. (a-c) represent coronal plane results for ROC of 5 mm, 6 mm, and 7 mm, respectively; (d-f) depict sagittal plane results for the same ROC values. Each subfigure maps frequency (1–6 MHz) along the horizontal axis and f-number (0.58–1.0) along the vertical axis. The pressure location is categorized into three zones: at the focus (yellow), at the lower skull bone (pink), and at the upper skull bone (blue).

4.5. The effect of the transducer design parameters on the side lobe

Side lobes higher than –10 dB in neuromodulation applications by t-FUS pose a significant risk of unintended acoustic energy deposition. The feature importance analysis, presented in Figure 7, reveals that frequency is the dominant contributor to side lobe suppression, with feature importance scores of 0.50 and 0.44 in the coronal and sagittal planes, respectively. This strong dependence highlights the central role of acoustic frequency in shaping the beam profile and suppressing off-target acoustic energy. Higher frequencies result in narrower focal zones and reduced diffraction, contributing to lower side lobe amplitudes. The f-number demonstrated a moderate influence on side lobe characteristics, with consistent importance scores of 0.39 across both anatomical planes. This finding aligns with physical intuition, as the f-number governs beam convergence; smaller f-numbers lead to tighter focusing, which can increase side lobe formation if not carefully balanced with aperture and frequency considerations. In contrast, ROC showed limited impact on side lobe suppression, with relatively low importance values of 0.11 and 0.17 in the coronal and sagittal planes, respectively.

4.6. The effect of the mouse skull on the acoustic field

From the preceding analysis, it becomes evident that skull morphology has a critical influence on transducer performance (pressure field properties). To further elucidate these effects, Figure 12 presents pressure field simulations for a representative transducer design (3 MHz, ROC = 5.75 mm, f-number = 0.575) under varying anatomical conditions. Figure 12(a) presents the case in which no skull bone is present. Here, the pressure field exhibits a sharply defined, symmetric elliptical focal

zone centered at the intended target, confirming the intrinsic focusing capability of the transducer in the absence of bone-induced aberration. Figure 12(b) isolates the effect of the upper skull bone, illustrating that while it does induce partial reflection and wavefront deformation, a well-defined elliptical focal region still emerges at the deep brain target with lower pressure magnitude. Figure 12(c) depicts the scenario in which the upper skull bone is removed and only the lower skull bone is present, allowing acoustic energy to transmit directly from water into soft tissue in the upper region of the coronal plane. As expected, reflections at the water–tissue interface are minimal; however, substantial reflection and scattering occur at the lower skull interface. In Figure 12(d), where both upper and lower skull bones are present, strong reflections are observed at both interfaces, significantly distorting the focal region. These results suggest that both upper and lower skull bones and the medium's homogeneity are essential considerations for accurate neuromodulation in preclinical t-FUS studies using mice. Failing to consider these factors may lead to unintended off-target stimulation, resulting in inaccurate outcomes and misleading interpretations.

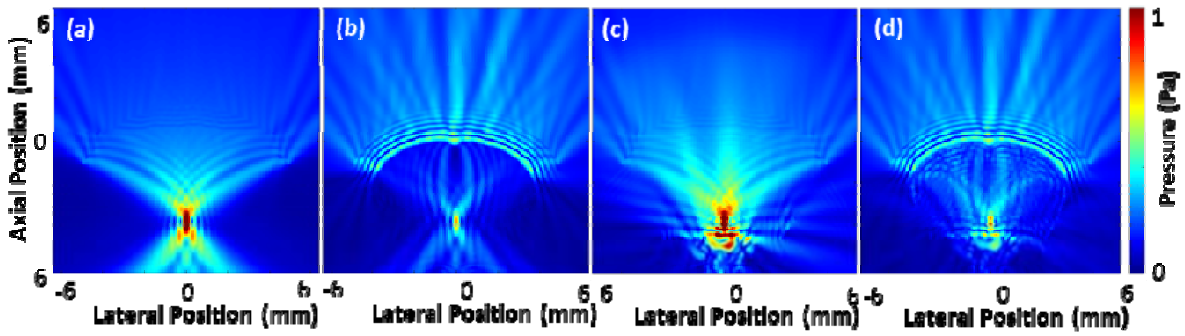

Figure 12. The effect of the mouse skull on acoustic wave propagation and focal region formation is demonstrated by comparing the pressure field of four cases in the coronal plane: (a) no skull, (b) the upper skull only, (c) the lower skull only, and (d) complete skull present.

5. Conclusion

In this study, we aim to design a single-element ultrasound transducer with optimal performance in deep-brain neuromodulation in a mouse model. A critical challenge in the deep-brain ultrasound intervention is that strong acoustic reverberation can be caused by the lower skull bone of mice, severely deteriorating the acoustic focus required for accurate energy delivery. To achieve an optimal design, we implemented a machine learning-based multi-objective optimization framework that combines an RF surrogate model with the NSGA-II algorithm. This approach enabled efficient exploration of the transducer design space (frequency, f-number, and ROC) against multiple performance evaluation criteria, including focal length, focal shape, maximum pressure at the focal region, location of the maximum pressure in the field, and side lobe suppression. The machine learning-based method employed in this study enables a computational analysis of how transducer design parameters and skull anatomy impact acoustic field characteristics, suggesting that frequency and f-number have a greater impact compared to ROC in designing a transducer for deep-brain neuromodulation. The optimized transducer design outperformed similar designs reported in the literature. In the meantime, the machine learning-based optimization method proposed in this study provides a framework for developing single-element ultrasound transducers that can achieve precise targeting with minimal off-target biological effects. This framework is adaptable and can be applied to design optimized transducers for targeting diverse brain regions in transcranial neurological interventions.

References

Airan R D and Butts Pauly K 2018 Hearing out Ultrasound Neuromodulation *Neuron* **98** 875-7

Angla C, Larrat B, Gennisson J L and Chatillon S 2023 Transcranial ultrasound simulations: A review *Med Phys* **50** 1051-72

Chen H, Deng T, Du T, Chen B, Skibniewski M J and Zhang L 2022 An RF and LSSVM–NSGA-II method for the multi-objective optimization of high-performance concrete durability *Cement and Concrete Composites* **129**

Darmani G, Bergmann T O, Butts Pauly K, Caskey C F, de Lecea L, Fomenko A, Fouragnan E, Legon W, Murphy K R, Nandi T, Phipps M A, Pinton G, Ramezanpour H, Sallet J, Yaakub S N, Yoo S S and Chen R 2022 Non-invasive transcranial ultrasound stimulation for neuromodulation *Clin Neurophysiol* **135** 51-73

Fini M and Tyler W J 2017 Transcranial focused ultrasound: a new tool for non-invasive neuromodulation *Int Rev Psychiatr* **29** 168-77

Garg A, Mukhopadhyay T, Belarbi M O and Li L 2023 Random forest-based surrogates for transforming the behavioral predictions of laminated composite plates and shells from FSDT to Elasticity solutions *Composite Structures* **309**

Ghanbari L, Rynes M L, Hu J, Schulman D S, Johnson G W, Laroque M, Shull G M and Kodandaramaiah S B 2019 Craniobot: A computer numerical controlled robot for cranial microsurgeries *Sci Rep-Uk* **9**

Ham H, Kim K S, Lee J H, Kim D N, Choi H J and Yoh J J 2024 Acoustic deep brain modulation: Enhancing neuronal activation and neurogenesis *Brain Stimulation* **17** 1060-75

He J, Zhu Y, Wu C, Wu J, Chen Y, Yuan M, Cheng Z, Zeng L and Ji X 2023 Simultaneous multi-target ultrasound neuromodulation in freely-moving mice based on a single-element ultrasound transducer *J Neural Eng* **20**

Hoa A M a D 2018 Labeled cross-sectional anatomy of the mouse on micro-CT.

Hou C, Wu Y, Fei C, Qiu Z, Li Z, Sun X, Zheng C and Yang Y 2022 An Optimized Miniaturized Ultrasound Transducer for Transcranial Neuromodulation *Front Neurosci* **16** 893108

Hu Z, Chen S, Yang Y, Gong Y and Chen H 2022 An Affordable and Easy-to-Use Focused Ultrasound Device for Noninvasive and High Precision Drug Delivery to the Mouse Brain *IEEE Trans Biomed Eng* **69** 2723-32

Hu Z, Yang Y, Ye D, Chen S, Gong Y, Chukwu C and Chen H 2023 Targeted delivery of therapeutic agents to the mouse brain using a stereotactic-guided focused ultrasound device *Star Protoc* **4** 102132

Huang L H, Kang J W, Chen G F, Ye W, Meng X Q, Du Q and Feng Z 2022 Low-intensity focused ultrasound attenuates early traumatic brain injury by OX-A/NF-κB/NLRP3 signaling pathway *Aging-Us* **14** 7455-69

Ilham S J, Kashani Z and Kiani M 2021 Design and Optimization of Ultrasound Phased Arrays for Large-Scale Ultrasound Neuromodulation *Ieee T Biomed Circ S* **15** 1454-66

Javid A, Ilham S and Kiani M 2023 A Review of Ultrasound Neuromodulation Technologies *Ieee T Biomed Circ S* **17** 1084-96

Jiménez-Gambín S, Jiménez N, Pouliopoulos A N, Benlloch J M, Konofagou E E and Camarena F 2022 Acoustic Holograms for Bilateral Blood-Brain Barrier Opening in a Mouse Model *Ieee T Bio-Med Eng* **69** 1359-68

Khan M R, Zekios C L, Bhardwaj S and Georgakopoulos S V 2021 Performance of Random Forest Algorithm in High-Dimensional Surrogate Modeling of Antennas. In: *2021 IEEE International Symposium on Antennas and Propagation and USNC-URSI Radio Science Meeting (APS/URSI)*, pp 1445-6

Kim Y G, Kim S E, Lee J, Hwang S, Yoo S S and Lee H W 2022 Neuromodulation Using Transcranial Focused Ultrasound on the Bilateral Medial Prefrontal Cortex *J Clin Med* **11**

King R L, Brown J R and Pauly K B 2014 Localization of ultrasound-induced in vivo neurostimulation in the mouse model *Ultrasound Med Biol* **40** 1512-22

Kobayashi Y, Azuma T, Shimizu K, Koizumi M, Oya T, Suzuki R, Maruyama K, Seki K and Takagi S 2018 Development of focus controlling method with transcranial focused ultrasound aided by numerical simulation for noninvasive brain therapy *Japanese Journal of Applied Physics* **57**

Kubanek J 2018 Neuromodulation with transcranial focused ultrasound *Neurosurgical Focus* **44**

Kyriakou A, Neufeld E, Werner B, Paulides M M, Szekely G and Kuster N 2014 A review of numerical and experimental compensation techniques for skull-induced phase aberrations in transcranial focused ultrasound *Int J Hyperther* **30** 36-46

Labib S, Bright R K and Liu J 2024 Focused Ultrasound in Cancer Immunotherapy: A Review of Mechanisms and Applications *Ultrasound Med Biol*

Lee J, Kim Y E, Lim J, Jo Y, Lee H J, Jo Y S and Choi J S 2024 Transcranial focused ultrasound stimulation in the infralimbic cortex facilitates extinction of conditioned fear in rats *Brain Stimulation* **17** 405-12

Lee W, Croce P, Margolin R W, Cammalleri A, Yoon K and Yoo S S 2018 Transcranial focused ultrasound stimulation of motor cortical areas in freely-moving awake rats *Bmc Neurosci* **19** 57

Lee W, Kim H C, Jung Y, Chung Y A, Song I U, Lee J H and Yoo S S 2016 Transcranial focused ultrasound stimulation of human primary visual cortex *Sci Rep-Uk* **6**

Legon W, Ai L, Bansal P and Mueller J K 2018a Neuromodulation with single-element transcranial focused ultrasound in human thalamus *Human Brain Mapping* **39** 1995-2006

Legon W, Bansal P, Tyshynsky R, Ai L and Mueller J K 2018b Transcranial focused ultrasound neuromodulation of the human primary motor cortex *Sci Rep* **8** 10007

Li X, Weng F, Sun W B, Liu R L and Xu H B 2020 Preliminary Research on Depression Treatment: Combination of Transcranial Magnetic Stimulation and MRI-Guided Low-Intensity Focused Ultrasound Pulsation *J Med Imag Health In* **10** 677-80

Liang B Y, Liu W, Zhan Q W, Li M C, Zhuang M W, Liu Q H and Yao J J 2019 y Impacts of the murine skull on high-frequency transcranial photoacoustic brain imaging *J Biophotonics* **12**

Liu Z, Kawabe T, Nishi T, Ito S and Fujiwara T 2024 Surrogate-Assisted Multi-Objective Optimization for Simultaneous Three-Dimensional Packing and Motion Planning Problems Using the Sequence-Triple Representation *Applied Artificial Intelligence* **38**

Macmanus D B 2023 Excision of whole intact mouse brain *Methodsx* **10**

Maria G D A, Dias N S, Nicolato R, de Paula J J, Bicalho M A C, Cunha R S, Silva L C, de Miranda D M, Viana B D and Romano-Silva M A 2024 Safety and efficacy of repetitive stimulation of the left dorsolateral prefrontal cortex using transcranial focused ultrasound in treatment-resistant depressed patients: A non-inferiority randomized controlled trial protocol *Asian J Psychiatr* **95**

Mehic E, Xu J M, Caler C J, Coulson N K, Moritz C T and Mourad P D 2014 Increased Anatomical Specificity of Neuromodulation via Modulated Focused Ultrasound *Plos One* **9**

Meng W, Lin Z, Bian T, Chen X, Meng L, Yuan T, Niu L and Zheng H 2024 Ultrasound Deep Brain Stimulation Regulates Food Intake and Body Weight in Mice *IEEE Trans Neural Syst Rehabil Eng* **32** 366-77

Murphy K R, Nandi T, Kop B, Osada T, Lueckel M, N'Djin W A, Caulfield K A, Fomenko A, Siebner H R, Ugawa Y, Verhagen L, Bestmann S, Martin E, Butts Pauly K, Fouragnan E and Bergmann T O 2025 A practical guide to transcranial ultrasonic stimulation from the IFCN-endorsed ITRUSST consortium *Clin Neurophysiol* **171** 192-226

Niu X D, Yu K and He B 2018 On the neuromodulatory pathways of the brain by means of transcranial focused ultrasound *Curr Opin Biomed Eng* **8** 61-9

Pang N, Huang X W, Zhou H, Xia X X, Liu X F, Wang Y B, Meng W, Bian T Y, Meng L, Xu L S and Niu L L 2021 Transcranial Ultrasound Stimulation of Hypothalamus in Aging Mice *Ieee T Ultrason Ferr* **68** 29-37

Pang N, Meng W, Zhong Y S, Liu X F, Lin Z R, Guo T X, Zhou H, Qi L, Meng L, Xu L S and Niu L L 2022 Ultrasound Deep Brain Stimulation Modulates Body Temperature in Mice *Ieee T Neur Sys Reh* **30** 1851-7

Pantea C, Osterhoudt C F and Sinha D N 2013 Determination of acoustical nonlinear parameter β of water using the finite amplitude method *Ultrasonics* **53** 1012-9

Samoudi M, Renterghem T V and Botteldooren D 2019a Computational modeling of a single-element transcranial focused ultrasound transducer for subthalamic nucleus stimulation *Journal of Neural Engineering* **16**

Samoudi M A, Van Renterghem T and Botteldooren D 2019b Computational modeling of a single-element transcranial focused ultrasound transducer for subthalamic nucleus stimulation *J Neural Eng* **16** 026015

Saper C B and Lowell B B 2014 The hypothalamus *Curr Biol* **24** R1111-6

Smith C S, O'Driscoll C and Ebbini E S 2022 Spatio-Spectral Ultrasound Characterization of Reflection and Transmission Through Bone With Temperature Dependence *Ieee T Ultrason Ferr* **69** 1727-37

Treeby B E and Cox B T 2010 k-Wave: MATLAB toolbox for the simulation and reconstruction of photoacoustic wave fields *Journal of Biomedical Optics* **15**

Treeby B E, Jaros J, Rendell A P and Cox B T 2012 Modeling nonlinear ultrasound propagation in heterogeneous media with power law absorption using a k-space pseudospectral method *Journal of the Acoustical Society of America* **131** 4324-36

Wang Q, Ding S L, Li Y, Royall J, Feng D, Lesnar P, Graddis N, Naeemi M, Facer B, Ho A, Dolbeare T, Blanchard B, Dee N, Wakeman W, Hirokawa K E, Szafer A, Sunkin S M, Oh S W, Bernard A, Phillips J W, Hawrylycz M, Koch C, Zeng H, Harris J A and Ng L 2020 The Allen Mouse Brain Common Coordinate Framework: A 3D Reference Atlas *Cell* **181** 936-53 e20

Zarhin D, Atsmon R, Ruggiero A, Baeloha H, Shoob S, Scharf O, Heim L R, Buchbinder N, Shinikamin O, Shapira I, Styr B, Braun G, Harel M, Sheinin A, Geva N, Sela Y, Saito T, Saido T, Geiger T, Nir Y, Ziv Y and Slutsky I 2022 Disrupted neural correlates of anesthesia and sleep reveal early circuit dysfunctions in Alzheimer models *Cell Rep* **38**

Zhang T, Pan N, Wang Y, Liu C and Hu S 2021 Transcranial Focused Ultrasound Neuromodulation: A Review of the Excitatory and Inhibitory Effects on Brain Activity in Human and Animals *Front Hum Neurosci* **15** 749162

Zhuang X, He J, Wu J, Ji X, Chen Y, Yuan M and Zeng L 2022 A Spatial Multitarget Ultrasound Neuromodulation System Using High-Powered 2-D Array Transducer *IEEE Trans Ultrason Ferroelectr Freq Control* **69** 998-1007